SLIDING MODE CONTROLLED THREE-PORT BOOST CONVERTER WITH PARTIAL POWER PROCESSING FOR ON-BOARD ELECTRIC VEHICLE CHARGERS

Mr. C.Brahmananda[1], B.Pravallika[2], V.Guru Mahesh[3], S.Arbaz Ahamad[4], P.Thrilok[5]

[1]Assistant Professor, Department of EEE, AITS, Kadapa

[2,3,4,5]Student (UG), Department of EEE, AITS, Kadapa

Abstract:

Using partial power processing (PPP) in the bidirectional DC-DC stage, this work aims to design and build a novel three-port boost AC-DC converter that enables on-board rapid charging for electric cars. The proposed three-port converter (TPC) significantly reduces charging time and allows higher-power operation without additional device stress, in contrast to conventional two-stage chargers that use a two-port AC-DC converter followed by a full-power-processing (FPP) DC-DC converter. The PPP-based DC-DC stage reduces power processing in the power conversion chain, which further improves efficiency. With its three distinct output voltage levels, the suggested TPC also reduces switching losses. To control the flow of power between the battery, AC, and DC connections, a Sliding Mode Controller (SMC) is utilized. With the SMC, the converter can be reliably controlled regardless of the load, grid voltage, or battery status. Its ability to withstand external disturbances and parameter uncertainties allows it to regulate the DC-link voltage precisely, operate at unity power factor on the AC side, and respond quickly to transient situations. As a result, the charging process is more reliable and the system is more stable overall. When PPP and the suggested SMC-based control strategy are used together, the DC-DC stage processes a fraction of the total power, which leads to smaller converters, lower costs, and reduced losses. This is in comparison to traditional two-stage FPP-based chargers, and this is true even without the use of soft-switching techniques. We use a MATLAB/Simulink-based model for 6.6 kW to assess the performance of the proposed charger under various operating situations.

I. INTRODUCTION

Quick and effective charging solutions, on par with traditional fuelling systems, are required due to the accelerated uptake of electric vehicles (EVs) [1]. Developing high-power on-board chargers is crucial since the charging speed is a big obstacle to EV adoption. But in traditional AC-DC topologies, getting a lot of power on board increases the size, rating, losses, and cost of the converter [2] – [4]. The two-stage architecture often used by conventional on-board EV chargers consists of an AC-DC converter with two ports and a DC-DC converter with full power processing (FPP), as seen in Figure 1(a) [5] - [8]. The DC-DC stage uses constant-current/constant-voltage (CC/CV) regulation to charge the batteries in such systems, while the AC-DC stage keeps the DC-link voltage (VH) constant. The AC-DC and DC-DC stages can be subjected to voltage stress levels of 400-600 V when fed single-phase AC inputs, which increases the size and cost of the device and limits its ability to operate at high power [9] - [11]. Overall efficiency is further reduced and bidirectional control becomes more complicated due to the requirement for high-current-rated components in the DC-DC stage [12] – [15]. A number of methods for improving efficiency have been suggested to overcome these restrictions; they include soft-switching, high-gain single/two-stage converters, and DC-DC stage partial-power processing (PPP) [16]-[18]. Although soft-switching does boost efficiency, the control complexity grows dramatically and peak values in FPP-based chargers stay between 93% and 96% [19]. By reducing the amount of power processed by the converter and increasing efficiency with fewer components, PPP lowers converter stress and improves battery life [20]. The proposed work incorporates a bidirectional PPP-based DC-DC stage with a three-port boost AC-DC converter, as seen in Figure 1(b). Although the DC-DC stage handles some power, the three-port converter (TPC) is responsible for immediately delivering the bulk of the power needed to charge the batteries. Charging efficiency is improved, devices may be made smaller, and strains on the switches are reduced as a result. The TPC further reduces switching losses by providing three separate voltage levels.

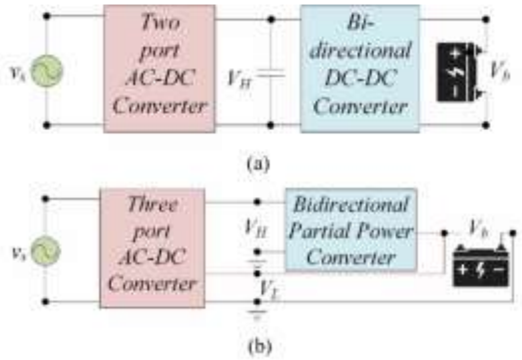

Fig. 1. General architecture of. (a) Conventional charger with FPP two-port converter, and (b) proposed fast charger with three-port converter. To achieve robust operation under variations in grid voltage, battery state-of-charge, and load demand, a Sliding Mode Controller (SMC) is proposed to regulate power flow among the AC, DC, and battery ports. The SMC ensures fast dynamic response, unity power factor at the AC side, and precise DC-link voltage regulation, while inherently tolerating parameter uncertainties and external disturbances. Integration of SMC with PPP ensures that only partial power is processed by the DC–DC stage, reducing losses, size, and cost, while enhancing overall system reliability and efficiency.

Main Contributions

1. Integration of a three-port boost AC–DC converter with PPP reduces the DC–DC stage rating while delivering high charging power.
2. Application of a Sliding Mode Controller provides robust and fast regulation of DC-link voltage, battery current, and AC power factor.
3. The proposed charger reduces switch voltage and current stress, switching losses, and component size, improving efficiency.
4. The combination of PPP and SMC allows for high-speed EV charging without the need for complex soft-switching techniques.

In summary, the proposed TPC with PPP-based DC–DC stage and SMC addresses the limitations of conventional two-stage chargers, offering higher efficiency, reduced cost, and faster charging suitable for on-board EV applications.

II. CIRCUIT CONFIGURATION, STEADY-STATE ANALYSIS, AND DESIGN

The proposed on-board EV charger consists of a three-port boost AC–DC converter (TPC) at the front-end, followed by a bidirectional buck–boost DC–DC converter with partial power processing (PPP), as shown in Fig. 2(a). The TPC comprises switches S_w, S_{wL}, diodes D_1, D_2, inductor L_i, and DC-link capacitors $C_H$and C_L. The bidirectional DC–DC stage consists of switches S_{b1}, $S_{b2}$and inductor L_b. For a single-phase 220 V system, the DC-link voltage $V_H$is regulated at 400 V, while the battery charging port $V_b$is controlled at 270 V.

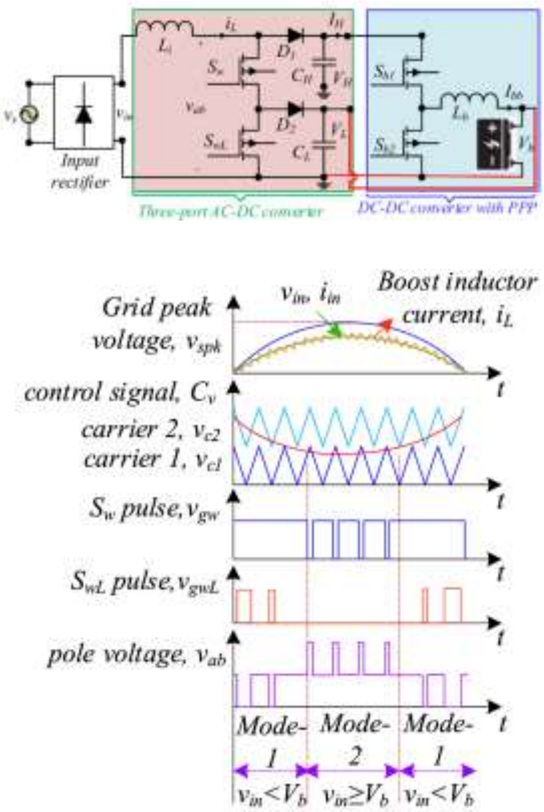

Fig. 2. Proposed PPP converter based fast charger and Pulse generation and switching waveforms.

The PPP architecture allows a direct transfer of power from the lower port $V_L$to the battery (bypass path, red line in Fig. 2(a)), while the DC–DC converter processes only a fraction of total charging power. Consequently, the charger can still supply the full battery charging power while significantly reducing the size, cost, and voltage/current stress on the DC–DC converter.

A. Modes of Operation

The TPC operates in two distinct modes:

Mode-1 ($V_{in} < V_b$):

- Switch $S_w$remains ON, and diode $D_1$is reverse-biased.
- **Switching state 1:** Inductor $L_i$stores energy through $S_w$and S_{wL}, while capacitor $C_L$supplies the battery directly (Fig. 3(a)).
- **Switching state 2:** Switch S_{wL}turns OFF, $S_w$remains ON, and diode D_2conducts, releasing energy from $L_i$to the battery (Fig. 3(b)).
- In this mode, the complete charging power is provided directly by the TPC.

Mode-2 ($V_{in} > V_b$):

- Switch S_{wL}remains OFF, while $S_w$switches ON and OFF.
- **Switching state 1:**$S_w$is ON, D_2conducts, and $L_i$stores energy through the voltage difference $V_{in} - V_b$(Fig. 3(c)).
- **Switching state 2:**$S_w$turns OFF, D_1conducts, and the battery receives charging power through $C_H$via the DC–DC stage (Fig. 3(d)).
- Charging power is shared between $C_H$and C_L, with most power still directly transferred via C_L.

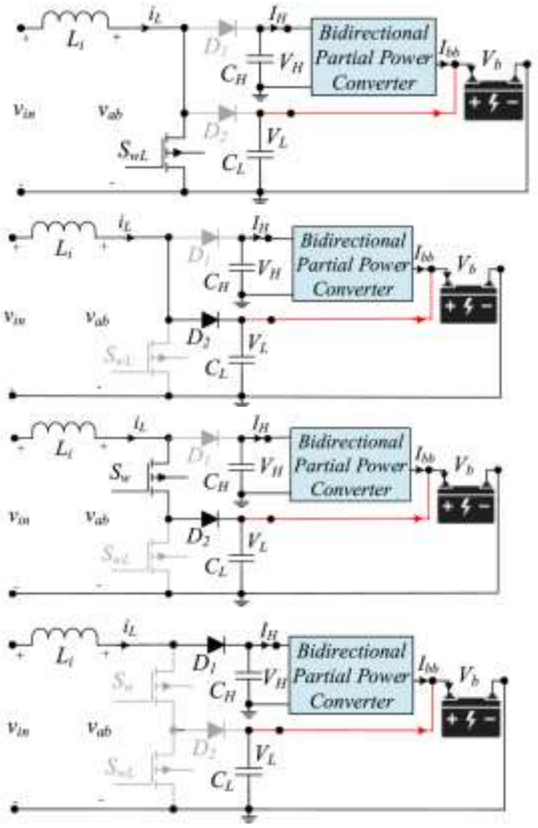

Fig. 3. Converter/Charger operation over one switching cycle during (a)–(b) Mode-1. (c)–(d) Mode-2.

B. Volt-Second Balance and Duty Ratios

Applying volt-second balance for the boost inductor L_i, the relation among V_{in}, V_b, and V_H for the two modes is:

$$V_{in} = \begin{cases} V_b(1-d_2), & \text{Mode-1} \\ V_b d_1 + (V_b + V_H)(1-d_1), & \text{Mode-2} \end{cases}$$

where d_1 and d_2 are the duty ratios of switches S_w and S_{wL}, respectively. These duty ratios are given by:

$$d_1 = \begin{cases} 1 - \dfrac{V_{in}}{V_b}, & \text{Mode-1} \\ 1 - \dfrac{V_{in} - V_b}{V_H}, & \text{Mode-2} \end{cases}$$

$$d_2 = \begin{cases} 1 - \dfrac{V_{in}}{V_b}, & \text{Mode-1} \\ 0, & \text{Mode-2} \end{cases}$$

For $V_s = 220$ V, $V_b = 270$ V, and $V_H = 130$ V, the duty ratio variations over a switching cycle are shown in Fig. 4(a). Only one high-frequency switch operates in each switching cycle.

C. Inductor Current Ripple

Considering a switching period T_s for TPC, the peak-to-peak current ripple in L_i is:

$$\Delta I = \begin{cases} \dfrac{V_{in}}{L} d_2 T_s, & \text{Mode-1} \\ \dfrac{V_{in} - V_b}{L} d_1 T_s, & \text{Mode-2} \end{cases}$$

Substituting (2) into (4):

$$\Delta I = \begin{cases} \dfrac{V_b}{L}(1-d_2) d_2 T_s, & \text{Mode-1} \\ \dfrac{V_H}{L}(1-d_1) d_1 T_s, & \text{Mode-2} \end{cases}$$

The maximum ripple occurs at $d_1 = 0.5$ or $d_2 = 0.5$, which aligns with the duty cycle variations shown in Fig. 4(a).

D. Power Transfer Analysis

Assuming lossless operation:

- Instantaneous input power:

$$p_{in}(t) = V_{in} I_{in} = \frac{V_p I_p}{2}(1 - \cos 2\omega t)$$

Power through C_H to DC–DC stage (Mode-2):

$$P_H = \int_{\arcsin(V_b/V_p)}^{\pi - \arcsin(V_b/V_p)} I_p \sin \omega t (1 - d_1) V_H \, d\omega t$$

Power directly transferred to battery:

$$P_L = \int_0^{\pi} p_{in} \, d\omega t - P_H$$

Fraction of direct power:

$$\beta_{\mathrm{dir}} = \frac{P_L}{\int_0^{\pi} p_{in} \, d\omega t} = \frac{2}{\pi} \arcsin \frac{V_b}{V_p} + \frac{V_b}{V_p} \cos \arcsin \frac{V_b}{V_p}$$

The fraction β_{dir} depends only on the ratio V_b/V_p and is independent of the DC-link voltage V_H.

E. Component Design

- C_L supplies battery charging current and can be an electrolytic capacitor.
- C_H mitigates high-frequency voltage ripples and is typically a film capacitor.
- Inductors L_i and L_b are designed considering maximum ripple current and duty ratios for both modes.

- DC–DC converter rating is reduced due to PPP, as it only processes a fraction of total power.

F. Sliding Mode Controller for TPC

A Sliding Mode Controller (SMC) is employed to regulate DC-link voltage V_H, battery current, and AC input current, ensuring:

1. Robust operation under input voltage variations.
2. Fast dynamic response for transient conditions.
3. Partial power processing efficiency by directing most power through the lower port.

The sliding surface is defined as:

$$s(t) = k_1(V_H^* - V_H) + k_2(I_b^* - I_b)$$

where $V_H^*$and $I_b^*$are reference DC-link voltage and battery current, and $k_1, k_2$are control gains. The switching law ensures:

$$u(t) = u_{eq} - K\,\text{sign}(s)$$

where $u_{eq}$is the equivalent control, $K$is the gain for robustness, and sign(s)provides discontinuous switching for fast convergence.

III. CONTROL STRATEGY

The control strategy of the proposed charger is designed to achieve unity power factor (UPF) operation while maximizing the power transferred directly through the TPC, thereby minimizing the power processed by the DC–DC stage. To achieve this, a dual-carrier pulse-width modulation (PWM) scheme is employed in combination with a Sliding Mode Controller (SMC) for robust regulation.

1. Mode-1 $(V_{in} < V_b)$: $C_v > v_{c1}$, where switch $S_w$remains **continuously ON**, and diode D_1stays **OFF**. Switch S_{wL}operates at high frequency, supplying the battery predominantly through the lower port C_L(single-stage conversion).

2. **Mode-2** $(V_{in} > V_b)$: $C_v < v_{c2}$, where switch $S_w$is **switched ON/OFF**, and S_{wL}remains **OFF**. In this mode, the battery receives power through **both the lower port (direct) and the DC–DC stage**, but the majority of power still flows directly via TPC.

The Sliding Mode Controller regulates the DC-link voltage $V_H$and battery current $I_b$while ensuring robust operation under grid voltage variations and load changes. The sliding surface is defined as:

$$s(t) = k_1(V_H^* - V_H) + k_2(I_b^* - I_b)$$

where $V_H^*$and $I_b^*$are reference DC-link voltage and battery current, and $k_1, k_2$are control gains. The control law is:

$$u(t) = u_{eq} - K\,\text{sign}(s)$$

Here, $u_{eq}$is the equivalent control for nominal operation, $K$is the gain for robustness, and sign(s)provides discontinuous switching to ensure fast convergence of the system to the desired operating point. The SMC ensures precise DC-link regulation, unity power factor, and fast transient response during supply or load variations.

IV. RESULTS AND DISCUSSION

The performance of the proposed charger is validated using MATLAB/Simulink under both steady-state and dynamic operating conditions for a rated supply voltage of 220 V, 50 Hz.

The device voltage stress across switches $S_w$and $S_{wL}$is 110 V $(V_H - V_b)$ and 290 V (for $V_b$at 60 % SOC), which is significantly lower than conventional two-stage FPP chargers (400–650 V).

The DC–DC stage processes only ~10 % of the total battery current (~2.3 A), while ~90 % of the power is delivered directly via the TPC, demonstrating the efficiency of PPP. The pulse waveforms confirm:

Mode-1: S_wON, S_{wL}switching

Mode-2: $S_w$switching, S_{wL}OFF

The three-level output voltage at the battery is observed (270 V–400 V–0 V), corresponding to the lower and upper port operation.

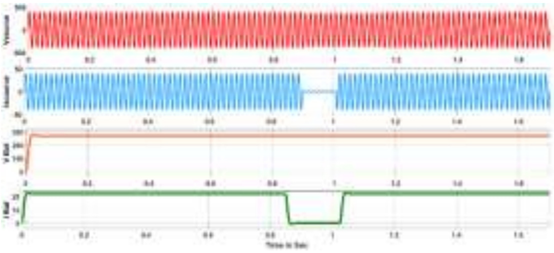

Fig. 4. Simulated Performance of proposed fast charger during change in vs (a) from 220 V−270 V, and (b) from 270 V−220 V.

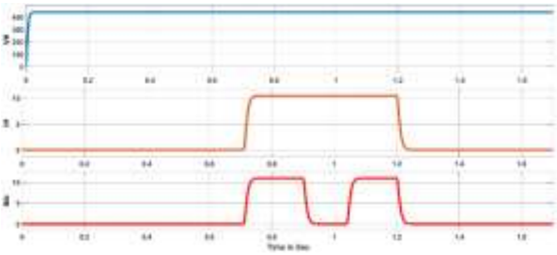

Fig. 5. Simulated performance of proposed fast charger during change in load i.e., Ib changes from full load to half load.

CONCLUSION

This paper presents a three-port boost AC–DC converter integrated with a bidirectional buck–boost DC–DC stage using partial power processing (PPP) for on-board fast EV charging. A Sliding Mode Controller (SMC) is implemented to regulate DC-link voltage, maintain unity power factor (UPF), and ensure robust operation under supply and load variations. The proposed charger achieves the following: High efficiency (~99.2 %) without requiring soft-switching due to the majority of power being delivered directly to the battery via TPC. Reduced device voltage and current stress compared to conventional two-stage full-power-processing (FPP) chargers, enabling higher charging currents with smaller switches. Robust performance under supply voltage fluctuations, load transients, and start-up/shut-down conditions due to the inherent robustness of the SMC. Significant reduction in DC–DC converter rating due to PPP, which lowers the size and cost of the charger. Three-level output voltage at the battery, minimizing switching losses and improving dynamic response. Simulation results validate that the proposed charger effectively combines high efficiency, compact design, fast charging capability, and robust control, making it a promising solution for next-generation EV on-board chargers.

REFERENCES

[1] F. Z. Peng, “A generalized unified power quality conditioner (GUPQC) for three-phase three-wire systems,” *IEEE Trans. Ind. Appl.*, vol. 37, no. 5, pp. 1300–1307, Sep./Oct. 2001.

[2] L. Ran, F. Z. Peng, and J. Wang, “Design of high-efficiency AC–DC converters for EV chargers,” *IEEE Trans. Power Electron.*, vol. 33, no. 8, pp. 7073–7085, Aug. 2018.

[3] Dr. P.Sankar Babu, K.Meenendranath Reddy and S.Sneha Madhuri. Improvement of Power Quality in Renewable Energy Integrated Microgrid System Using CMBC. International Journal for Modern Trends in Science and Technology 2021, 7 pp. 299-303.

[4] S. Sharma, R. K. Gupta, and P. K. Ray, “Two-stage bidirectional EV charger with full-power DC–DC conversion,” *IEEE Trans. Ind. Electron.*, vol. 66, no. 5, pp. 3607–3617, May 2019.

[5] H. Abu-Rub, M. Malinowski, and K. Al-Haddad, *Power Electronics for Renewable Energy Systems, Transportation and Industrial Applications*, Wiley, 2014.

[6] W. Xiao, Y. Xing, and Z. Li, "Single-stage EV charger using high-gain AC–DC conversion," *IEEE Trans. Ind. Appl.*, vol. 55, no. 3, pp. 2341–2350, May/June 2019.

[7] K.Meenendranath Reddy, & Syed Reshma. (2022). A Comparative Analysis of Integrated DC Microgrid with Hybrid Power Generation Systems by an Intelligent Control Strategy. International Journal of Recent Research in Electrical and Electronics Engineering, 9(2), 1–10.

[8] Ganji, M. (2025). Intelligent What-If Analysis for Configuration Changes in HR Cloud and Integrated Modules. International Journal of All Research Education and Scientific Methods, 13(04), 4828–4835. https://doi.org/10.56025/ijaresm.2025.1304254828.

[9] Marella, V. C., Veluru, S. R., & Erukude, S. T. (2025, September). FedOnco-Bench: A Reproducible Benchmark for Privacy-Aware Federated Tumor Segmentation with Synthetic CT Data. In 2025 4th International Conference on Innovative Mechanisms for Industry Applications (ICIMIA) (pp. 870-876). IEEE.

[10] Henry Cyril. (2025). AI-DRIVEN ANOMALY DETECTION, OUTAGE PREDICTION, AND SELF-HEALING IN TELECOM PROVISIONING SYSTEMS. International Journal of Applied Mathematics, 38(12s), 2817–2832. https://doi.org/10.12732/ijam.v38i12s.1589.

[11] Kalyan, R. ., Subbaiah, M. V. ., Charan, B. S. ., Reddy, K. M. ., & Babu, D. P. S. . (2022). Modelling and Control of SEPIC and BIDC Converter Based off-Board EV Battery Charger using PV Array. *Journal of Energy Engineering and Thermodynamics*, *2*(04), 36–45.

[12] C. Cecati, G. Spagnuolo, and F. Ciancetta, "Control strategies for three-port converters in EV fast chargers," *IEEE Trans. Ind. Electron.*, vol. 62, no. 5, pp. 3083–3092, May 2015.

[13] Y Doragacharla, V. R. (2026). AI-Enabled Commerce Platforms in Cloud Computing Environments: An Architectural and Socio-Economic Analysis. Journal of Computational Analysis & Applications, 35(1).

Trans. Veh. Technol., vol. 68, no. 8, pp. 7473–7484, Aug. 2019.

[14] Kavitha, K. ., Reddy, K. M. ., & Babu, D. P. . (2022). An Improvement of Power Control Method in Microgrid Based PV-Wind Integration of Renewable Energy Sources. *Journal of Energy Engineering and Thermodynamics*, *2*(06), 18–28.

[15] Srinivasa Kalyan Immadi. (2025). Harnessing Artificial Intelligence In Oracle Hcm: Revolutionising Workforce Management With Automation And Predictive Analytics. International Journal of Data Science and IoT Management System, 4(4), 7–13. https://doi.org/10.64751/ijdim.2025.v4.n4.pp7-13.

[16] Sai Maneesh Kumar Prodduturi. (2025). EFFICIENT DEBUGGING METHODS AND TOOLS FOR IOS APPLICATIONS USING XCODE. International Journal of Data Science and IoT Management System, 4(4), 1–6. https://doi.org/10.64751/ijdim.2025.v4.n4.pp1-6.

[17] S. Buso, F. Crescimbini, and G. Spiazzi, "Partial power processing converters for photovoltaic and EV applications," *IEEE Trans. Power*

Electron., vol. 29, no. 5, pp. 2389–2398, May 2014.

[18] H. Li, W. Xiao, and Z. Qian, "Three-port AC–DC converter with SMC for robust EV battery charging," *IEEE Trans. Ind. Appl.*, vol. 58, no. 4, pp. 1582–1593, July/Aug. 2022.

[19] S. Madan Gopal, & K. Meenendranath Reddy. (2023). Design and Control of High Voltage Gain Interleaved Boost Converter for Fuel Cell Based Electric Vehicle Applications. *Journal of Electronics, Computer Networking and Applied Mathematics* , *3*(02), 9–24.

[20] F. Z. Peng, "A generalized approach to partial power processing for EV and renewable applications," *IEEE Trans. Ind. Electron.*, vol. 65, no. 2, pp. 1234–1244, Feb. 2018.